The Missing Baryon Component: A search for the Cosmic Web using the CMB

Mitchell de Zylva

Supervised by
Dr Chrisitan Reichardt

School of Physics
Faculty of Science
University of Melbourne

October 30, 2019

Submitted in fulfillment of the requirements of the degree of
Master of Science (Physics)

Statement of contribution:

This is to certify that:

- This thesis entitled "The Missing Baryon Component: A search for the Cosmic Web using the CMB" comprises only my original work except where indicated otherwise.
- Due acknowledgement has been made in the text to all other material used.
- The thesis is no longer than 50 pages in length, inclusive of tables, figures, bibliographies and appendices.

.....

Mitchell de Zylva

Acknowledgements:

I would like to dedicate this thesis to my father, without whom I would not have made it through this

It matters not how strait the gate,
How charged with punishments the scroll,
I am the master of my fate,
I am the captain of my soul.

Abstract

Abstract goes here..

Contents

Chapter 1

Introduction

1.1 Modern Cosmology, and the Cosmic Microwave Background

The basis for modern cosmology relies on several fundamental assumptions stemming from observation, the chief of which is the Big Bang Model. Following Hubble's discovery of a relation between distances to galaxies and their recessional velocities, the *Copernican Principle* leads to the conclusion that in the past, objects in the universe were much closer together. His observations gave rise to the Lemaitre's Hubble Law,

$$v \propto d \tag{1.1}$$

This suggests that at some point in the past, the universe was much smaller than it is at present, the conservation of energy then implies that at some point in the past, the universe must have been an incredibly hot, dense environment. Using general relativity, the extrapolation backwards in time yields a singularity of infinite density and temperature, which is commonly called the *Big Bang*

Another assumption stemming from observation is that of isotropy. Based on observation, there appears to be no favoured direction in the universe, since distributions of distant galaxies and other extragalactic sources seem to be evenly distributed across the sky. Perhaps the most spectacular example of this isotropy is the presence of the *Cosmic Microwave Background*.

Discovered in 1964 (Penzias & Wilson, 1965), it was noticed that there was isotropic black-body radiation at $T \approx 2.7\,\mathrm{K}$. Since the peak of this radiation is in the microwave section of the electromagnetic spectrum, it was termed the *Cosmic Microwave Background*.

The Cosmic Microwave Background (CMB) is a near-perfectly uniform field of background radiation, which as its name suggests, sits primarily within the microwave part of the electromagnetic spectrum. It is the closest measurement we have to a perfect black-body, with variations to approximately one part in 100000, with an RMS of $18\,\mu\mathrm{K}$ Wright (2004).

Theory holds that a very short time after the Big Bang ($\sim 10^{-37}$ seconds), the universe underwent an exponential growth period now termed *inflation*. This phase is necessary to ensure that the universe is isotropic, whilst also still taking into account the apparent causal disconnect between different edges of the universe. During this period, the universe was smoothed out, only leaving behind irregularities that originated with quantum fluctuations in the scalar field that drove it. These irregularities are what eventually gives rise to the large scale structure of the universe.

As the universe adiabatically cooled, there was a considerable period of time, until approximately 380000 years after the Big Bang, where photons were coupled to the other components of

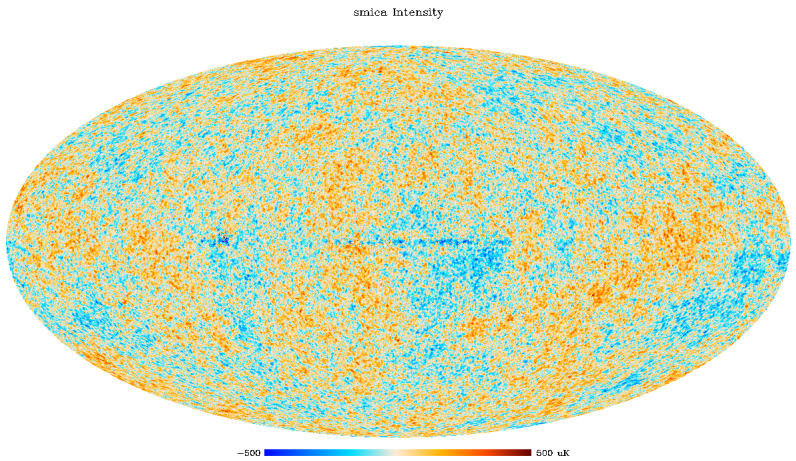

Figure 1.1: *Planck* Satellite Full Sky CMB Map

the universe, such as the baryonic and dark matter. This period is what allowed for the quark-gluon plasma to mix appropriately, and develop sound waves, ultimately resulting in the characterstic pattern in the CMB. This pattern is highly dependant on statistical parameters, and so the characterisitic angular size of the pattern of the CMB is incredibly sensitive to the relative proportions of the universe's matter-energy density. These charactersitic angular splotches can be decomposed into a power spectrum, which exibits a shape highly dependant on universal parameters.

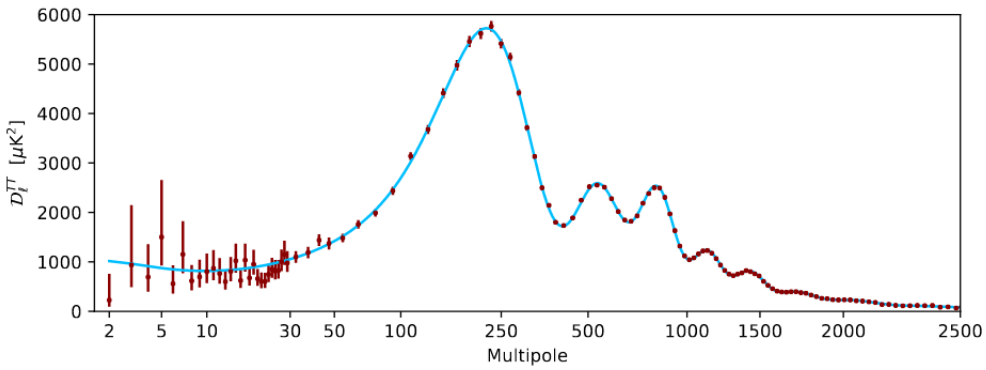

Figure 1.2: *Planck* 2018 Angular Power Spectrum (Planck Collaboration et al., 2018)

The Cosmic Microwave Background (CMB) provides the most accurate and detailed measures of the primary cosmological parameters to date.

1.2 Cosmological Parameters

For a Λ CDM universe, there are six independant paramters which descirbe the evolution and behaviour of the universe, the physical baryon density $\Omega_b h^2$, the physical dark matter density $\Omega_c h^2$, the age of the universe t_0 (or its reciprocal, the Hubble constant H_0), the scalar spectral index n_s, the curvature fluctuation amplitude Δ_R^2, and the reionisation optical depth τ.

Currently, the highest precision measures of these features from the CMB come from Planck Collaboration et al. (2018), which details that baryonic matter only comprises $\approx 5\%$ of the universe's energy density. In principle, this component of the universe should be directly measurable. At just

three minutes after the Big Bang, deuterium can be used as a tracer for this abundance (Steigman, 2007), and at redshift $z \geqslant 2$, the baryon fraction can be found in the absorption lines of quasars passing through the diffuse, photo-ionised intergalactic medium, known as the Lyman-α forest (Weinberg et al., 1997). However as the universe evolved, this gas became sparser as it became more ionised. This makes searching for the entirety of the baryon fraction at low redshift difficult. When this fraction is calculated directly from observations, it shows only one tenth of the baryonic content shown in high redshift measurements is contained in galactic structures (Persic & Salucci, 1992). Some revised estimates considered that the limitations of observations were primarily to blame for this discrepency, and not inherent new physics (Bristow & Phillipps, 1994; Fukugita et al., 1998)

The baryon content has been confirmed to a very high accuracy with recent CMB experiments, first with the *Wilkinson Microwave Anisotropy Probe* (WMAP) (Spergel et al., 2007), and then with the *Planck* Satellite (Planck Collaboration et al., 2018). When we quote quantities, we take values from the latest *Planck* paper

Parameter	Value	Error
$\Omega_c h^2$	0.120	± 0.001
$\Omega_b h^2$	0.0224	± 0.0001
n_s	0.965	± 0.004
τ	0.054	± 0.007
$100\Theta_\star$	1.0411	± 0.0003
H_0 (km s^{-1} Mpc^{-1})	67.4	± 0.5

Chapter 2

The Missing Baryon Problem

The Missing Baryon problem is one that arises when we try and make an account of the baryons at low redshift. At high redshift ($z > 2$), the Lyman-α forest provides a good measure of the proportion of baryons, since at these redshifts the majority of the baryons in the universe are contained in diffuse gas. These analyses give a reported value

$$\Omega_{baryon} \geq 0.035$$

Observed light-element ratios and standard nucleosynthesis allows for direct computation of the expected baryon densities, which is in agreement with the above figure (Burles & Tytler, 1998)

$$\Omega_{baryon} = (0.019 \pm 0.001)h^{-2} = 0.039 \pm 0.002$$

The agreement between these two measures of baryon density, and the measurement obtained from the CMB lends confidence to the value obtained.

However, at low redshifts, all analysis indicates that the summing over all observed contributions gives a value of

$$\Omega_{\star} + \Omega_{HI} + \Omega_{H_2} + \Omega_{X-Ray,cl} \approx 0.0068 \leq 0.011$$

This severe discrepency between measurements at high and low redshifts suggests that either the majority of the baryons at low redshifts are yet to be detected, or there are fundamental errors in numerous independant measures of the baryon density at high redshift.

2.1 Stellar Baryons

The most obvious location to search for baryons are in the stellar populations of galaxies. At a broad level, we can imagine that there are two distinct stellar populations which can be considered to be found in high density galaxies; a class of old stars which exists in the spheroidal region of a galaxy, and a class of young stars in the disk region, as well as a third population existing in irregular galaxies.

Estimating the proportion of stellar baryons therfore becomes an exercise in galactic morphology and luminosity density function computation. There are three primary classes of stars which need to be considered, stars contained in the central disk of the galaxy, starts contained in the bulge (spheroid), and starts contained in irregular galaxies, which don't conform to simple catergorical definitions. Perfoming this calculation gives mean mass density numbers for these three

classes of stars gives

$$\Omega_{\text{Spheroid Stars}} = (0.00180^{+0.00121}_{-0.00085})h^{-1}$$
$$\Omega_{\text{Disk Stars}} = (0.00060^{+0.00030}_{-0.00024})h^{-1}$$
$$\Omega_{\text{Stars in Irregular Galaxies}} = (0.000048^{+0.000033}_{0.000026})h^{-1}$$

These numbers depend on the mass-to-light ratio for age estimation, and so in turn are dependant on the cosmological parameters in a complex way. Even if efforts were made to remove this dependancy by changing the methodology used to calculate the mass-to-light function, the necessity for the new methodology to hold consistent with other measurements would force the dependancy regardless.

2.2 Cold Interstellar Medium

We also know that some of the baryons in the local universe are stored in the Cold Interstellar Medium. The cold interstellar medium is a term for neutral and molecular gas, primarily consisting of unionised hydrogen gas (HI). The HI present in gas-rich galaxies is the best tracer for the neutral hydrogen mass content in the near universe, since it can be shown that very little neutral gas is present in objects outside the galaxy population in these regions. At redshift $z \approx 0$, there have not been any free HI clouds detected by radio surveys that have not yet subsequently been detected in optical bands (Rao & Briggs, 1993) , and so optical detection in galaxies can be considered to be adequate when taking a census of the total baryons contained in the cold interstellar medium.

The HI content of a given galaxy can be calculated from the optical luminosity functions of given galaxy morphological types. For a given optical luminosity function $\phi^T(M)$, and a given HI mass content $M^T_{HI}(M)$, as functions of absolute magnitude M, the total HI mass content of a given galaxy morphological type T can be found by computing an integral over all luminosities

$$M_{HI} = \int \phi^T(M) M^T_{HI}(M) dM$$

Adding all the contributions for all morphological types will therefore give an estimate of the total HI at $z = 0$. At these distances, spiral galaxies are the primary contributors to the neutral hydrogen content, with 89% of the hydrogen mass found in types later than S0 spiral galaxies. Initial estimates (Rao & Briggs, 1993) place the mass density of neutral hydrogen at $z = 0$ at

$$\Omega_{HI} = (2.5 \pm 0.6) \times 10^{-4} h_{75}^{-1}$$

Later surveys, such as the HI Parkes All-Sky Survey (HIPASS), refined this measurement further (Zwaan et al., 2003). HIPASS is a blind survey of the southern sky south consisting of approximately 7000 galaxies. The much higher number of galaxies in this survey necessitated a different method of computing the neutral hydrogen fraction. Taking a statistical approach, and assuming that the survey is inherently not detecting neutral mass fraction below a certain magnitude, the probability that a galaxy with a given HI mass is

$$p(M_{HI,i}|D) = \frac{\Theta(M_{HI,i})}{\int_{M_{HI,\lim(D_i)}}^{\infty} \Theta(M_{HI}) dM_{HI}}$$

, where $M_{HI,\lim(D_1)}$ is the minimum detectable HI mass at some distance D_i. This essentially gives the fraction of galaxies in the survey with a given HI mass sufficient to be detected. The parent distribution Θ can then be maximised by finding which product of probabilities is also

maximal. The statistical nature of this method requires accounting for various forms of bias, such as selection bias in the survey, the Eddington effect, self-absorption of the neutral hydrogen, and cosmic variance. This methodology gives a measure of the mass density as

$$\Omega_{HI} = (3.8 \pm 0.6) \times 10^{-4} h_{75}^{-1}$$

2.3 Photoionised Lyman α

At higher redshifts, the entirety of the baryon content in the universe can essentially be found in large quanties of gas that have not yet collapsed into galaxies, which shows up very clearly in the Lyman α (Lyα) forest. At low redshifts, we can search for the residual Lyα signal using HI absorber frequencies in distant quasars. By making the assumption that these absorbers are isothermal spheres, and choosing a given impact parameter, the total cloud mass can be essentially inferred from the HI column density.

One model for estimating the contribution of the local Lyman α forest is outlined by Penton et al. (2000). From big bang nucleosynthesis, the total baryons contributed from the low-z Lyα is given by

$$\Omega_{Ly\alpha} = \int_{N_{min}}^{N_{max}} \frac{\phi_0(N_{HI}, p) M_{cl}(N_{HI}, p, J_0)}{\rho_{crit}} dN_{HI}$$

, where $M_{cl}(N_{HI}, p, J_0)$ is the mass of an individual cloud , $\phi_0(N_{HI}, p)$ is space density of the clouds, N_{HI} is the column density of the clouds, J_0 is the specific intensity of the metagalactic ionizing radiation field ,$\rho_{crit} = 3H_0^2/8\pi G$ is the critical density at the present day which is necessary to halt the expansion of the universe.

Making more assumptions about the compostion of the spheres, and that the gas is in photoionising equilibrium, the impact parameter, this reduces the integral to

$$\Omega_{Ly\alpha} = (0.008 \pm 0.001) \left[J_{-23} p_1 00 \left(\frac{4.8}{\alpha_s + 3} \right) \right]^{1/2} h_{70}^{-1}$$

, where α_s is the spectral index of the radiation field, $J_{-23} = J_0/10^{-23}$, $p_{100} = p/(100kpc)$ and $h_{70} = H_0/(70Mpc)$. This corresponds to approximately 20% of the baryons, but it inherently makes a number of rather significant assumptions, which are highly dependant on the number of Lyman α absorbers detected at low redshifts.

Further accounting for the fact that the clouds are gravitationally bound, and that their densities are typical over a characteristic Jeans length allows for further refinement of this number (Schaye, 2001). Doing so yields a measure of the number of baryons in the residual Lyman α forest of $\Omega_{Ly\alpha} = 29\% \pm 4\%$ (Penton et al., 2004; Danforth & Shull, 2008)

2.3.1 OVI and BLA Absorbers

Because gas at low redshift exists at a large range of temperatures, and at a higher metalicity that the same gas at higher redshifts, distant quasars will exhibit absorption from higher Lyman alpha lines, such as oxygen (OVI), and broad Lyman α lines. The OVI absorption line probes gas in temperature ranges from 10^5 - 10^6 K, which has been shock heated as a result of gravitational instability during structure formation. Gas hotter than this is only sensitive to very weak absorption lines from higher ions, such as O VII, O VIII, Ne X, N VI, and N VII, which are only detectable in weak X-Rays (Danforth & Shull, 2005).

Broad Lyman α also act as a tracer of the gas in these temperature ranges. Theory suggests that the ionisation equilibrium of gas should contain a very small portion of neutral gas, typically

$f \sim 10^{-5} - 10^{-6}$, so there should be some Ly α emission, thermally broadened by the intervening gas (Richter et al., 2006). It is not entirely clear if the OVI and BLA absorbers trace the same underlying gas phase, so they have been included here together.

The method of calculating these numbers is a comparatively simply integral, over the number of absorbers per redshift bin, $dN_{OVI,BLA}/dz$. This does make several assumptions which are sensitive to the visibility, as well as the number of absorbers in a given survey.

Danforth & Shull (2005) found the proportion of matter contained in OVI absorbers to be approximately 5%, extrapolated from ~ 50 absorbers. However, this number is highly dependant on model-dependant spread of oxygen/hydrogen metalicities, the redshift range of the survey, and OVI ionisation fractions, leading to large errors on this measurement.

Richter et al. (2006) found the proportion from BLAs to be $\sim 15\% - 150\%$ of the total baryon fraction, from a sample of between 20 and 50 sources. The reason for the large uncertainty is the inherent uncertainty in the detection of BLA sources. In fact, the unreasonably high measurement of the baryon fraction says that this method is inherently counting sources which are not actually good tracers of the free baryons. There is also some confusion regarding sources which appear as both OVI and BLA absorbers, since the connection between the two types are not clear.

2.4 Summary

These methods all carry some sources of error with them, some so large that they call into question their validity entirely. These errors stem from the underlying assumptions assosciated with their method of calculation, as well as the inherent difficulty of detection for some methods. If we include some smaller contributions, such as from cluster contributions ($\Omega_b^{(cl)} \sim 4\%$)(Fukugita & Peebles, 2004) , or the circumgalactic medium ($\Omega_b^{(CGM)} \sim 5\% \pm 3\%$), and account for the possiblity that these techniques probe the same phase space, these still do not account for the entirety of the baryon component known from the CMB.

Chapter 3

The Warm-Hot Interstellar Medium

High resolution hydrodynamical simulations allow us to predict the overall structure of the cold dark matter in the universe (Cen & Ostriker, 1999, 2006; Smith et al., 2011; Davé et al., 2001). These can in turn be used to estimate the baryon distribution at low and moderate redshifts.

It is clear that by the current era, heirachical structure formation collects baryons in gravitational potential wells formed by the dark matter, which moves a significant portion of the baryon component that was previously located in the intergalactic medium at higher redshifts, into structure, such as stars, galaxies, groups, and clusters.

These simulations indicate that the baryons at low redshift fall into four general phases, defined by the overdensity $\delta \equiv \rho/\bar{\rho} - 1$ (where $\bar{\rho}$ is the mean density of baryons).

- Diffuse Gas: $\delta < 1000$, $T < 10^5 K$, Photoionised gas which is visible in Lyman-α absorption spectra
- Condensed: $\delta > 1000$, $T < 10^5 K$, Stars and cool galactic gas
- Hot: $T > 10^7 K$, Galaxy Clusters and Groups
- Warm-Hot: $10^5 K < T < 10^7 K$, Warm-Hot Intergalactic Medium (WHIM)

Simulations (Cen & Ostriker, 1999; Davé et al., 2001) indicate that at redshift $z = 0$ approximately $30 - 40\%$ of baryonic mass is contained within the last catergory, in the WHIM. WHIM gas seems to primarily trace filamentary large scale structures, and clusters around sites of galaxy formation. Because the gas is not bound or virialised, it is apparent that the mechanism which heats it to such high tempratures is shock-heating, caused by gas acreting onto large scale structure. This is consistent with measurements from the soft X-ray background.

Because the temperature and density of the WHIM are correlated, and the WHIM is in turn correlated with the large scale structure, we can use the precense of other tracers of large structure, temperature, and density to search for the baryons contained in the WHIM.

The WHIM is considered to exist in a filamentary web, which has been shock-heated during the process of structure formation to the temperatures described above. It is so highly ionised, and so disperse (with average densities of the order of 10 particles per cubic meter), that they can only emit or absorb far-ultraviolet or soft x-ray photons. These photons are primarily at highly ionised lines of C, O, Ne, and Fe (Cen & Fang, 2006).

Tracking the baryons contained in the WHIM can only be done by exploiting both experimental multiwavelength observations and theoretical calculations. X-Ray and UV spectroscopic surveys

measure the mass of WHIM using the relative and absolute metal content, and the ionisation correction. These can be then combined with optical and infrared photometry and spectroscopy which measure dark matter concentrations by measuring galaxy density around WHIM filaments. These observations then feed into simulations, which allow for more detailed study of virialised structure and the intergalactic medium.

The intensity of the signals obtained from direct observation is low in both the UV and the X-Ray bands, both as a result of the density and the relatively small size of the filaments (1 - 10 Mpc). Direct detection ideally requires large field of view and effective area imager-spectrometers, which is not currently available. The strategy that can best be utilised with current technology involves searching for discrete absorption lines in the spectra of bright, featureless background astrophysical sources.

The key feature necessary to detect an absorption line is the ratio between the line wavelength and its equivalent width, called its transition contrast. For the dominant absorption lines of oxygen, in this case OVI, the current resolving power of UV spectrometers is sufficient to measure its transition contrast, but for the X-Ray band, it is worse, and so searches for the WHIM have proven more fruitful in the UV band than in the X-Ray (Danforth & Shull, 2005; Richter et al., 2006). Using hydrodynamical simulations to replicate the observed absorption per unit redshift, it can be shown that if the WHIM was based solely on the OVI absorption, it would only account for approximately 10 percent of the missing baryon component.

An alternative method for searching for the missing mass is to look for hydrogen absorption in broad Ly-α absorbers (BLAs). At the temperatures that the WHIM is thought to exist at, most of the hydrogen will be ionised, but left-over neutral hydrogen can still imprint Lyman series absorption onto the ultraviolet spectra of background objects. These lines will be be very broad, given that the temperatures of the WHIM create a Doppler parameter of the order of $b \approx 40\,\mathrm{km/sec}$. This technique again gives a similar measurement to that done with OVI absorbers, and so suggests that BLAs and OVI absorbers can be considered to be good tracers of the WHIM, but aren't sufficient to probe the entirety of the missing mass due to the majority of it existing in temperatures only probed by the X-Ray band.

Comprehensive studies of the WHIM therefore require both the UV and X-Ray bands, since the X-Ray is crucial to detect the WHIM, and provide an accurate ionisation correction, and the UV is necessary to measure the assosciated amount of HI and hence the baryonic mass of the system.

According to theory, the chances of finding a WHIM filament along an arbitrary line of sight increases with the path length crossed between the observer and the beacon used to obtain the X-Ray images of intervening space, and the inverse of the baryon column density in the filament in question. This tells us that the larger the amount of baryons in the filament, the lower the probability of finding one. It can be shown that the detection of the WHIM is within the range of instrumentation currently, but it requires long observation times, making it untenable. Searching for an alternative tracer for the WHIM is therefore necessary to accurately locate the missing baryon content.

Chapter 4

The Sunayev-Zeldovich Effect

4.1 Atomic Physics

The thermal Sunyaev-Zel'dovich effect is one possible tracer. Sunyaev-Zel'dovich effect is one type of spectral distortion in the CMB, one which refers to the inverse compton scattering of CMB photons off of hot electrons in the WHIM. In order for a spectral distortion to exist in the CMB, it must occur sufficiently late in the cosmological timeline that the radiation doesn't thermalise and regain a pure Planck spectrum (approximately $z < 2700$).

Compton Scattering is a form of inelastic scattering between light and free charged particles, such as electrons. There is a momentum transfer between the photon in the interaction, and the charged particle, and so the photon's wavelength changes as a result of the scattering.

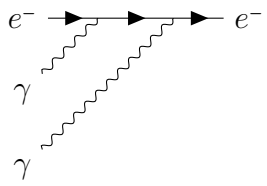

Figure 4.1: S-Channel Feynmann Diagram for Compton Scattering

It was first described in the context of X-rays interacting with electrons in atoms (Compton, 1923), and so regular Compton Scattering is taken to describe the interaction between a high energy photon, and a low energy particle. By applying principles of conservation of momentum, and conservation of energy, the formula for the shift in wavelength as a result of this scattering is given by

$$\Delta\lambda = \frac{h}{m_e c}\left(1 - \cos\theta\right) \tag{4.1}$$

where m_e is the mass of the electron, and θ is the angle between the incident and scattered trajectories.

For the Sunyaev-Zel'dovich effect however, the energies of the photons in question are much lower than the energies of the electrons involved, so the frequency shift is parametrised by something called the Compton y-parameter. The full expression for the Compton y-parameter is

$$y = \int \frac{k_B T_e}{m_e c^2} n_e \sigma_T dl \tag{4.2}$$

where $m_e c^2$, k_B, and σ_T are the electron rest mass energy, Boltzmann constant, and Thompson Cross Section respectively. These are all well defined constants, and so have no effect on the integration. The y-parameter therefore amounts to the line-of-sight integration over $n_e T_e$, which are the electron gas density and temperature. The degeneracy between temperature and pressure can be broken in principle by obtaining measurements of one of the two quanties, which we in princple take from hydrodynamical simulations.

This y parameter can be calculated in the CMB from frequency information. Starting from Kompaneets equation (Kompaneets, 1957), the time rate of change of the photon occupation number $\bar{n}$ due to Compton Scattering by non-relativistic, isotropic Maxwellian electron gas is given by a non-relativistic Fokker-Planck Equation (Rephaeli, 1995)

$$\frac{\partial \bar{n}}{\partial t} = \frac{kT}{mc}\frac{\sigma_T n_e}{x^2}\frac{\partial}{\partial x}\left[x^4\left(\frac{T_e}{T}\frac{\partial \bar{n}}{\partial x} + \bar{n} + \bar{n}^2\right)\right] \tag{4.3}$$

where $x = h\nu/kT$ is the non-dimensional frequency, T is the temperature of the radiation, n_e and T_e are the number density and temperature of the electrons, and σ_T is the Thompson cross section. Because $T_e >> T$, the first term in the parenthesis dominates, reducing the above to

$$\frac{\partial \bar{n}}{\partial t} = \frac{kT_e}{mc}\frac{\sigma_T n_e}{x^2}\frac{\partial}{\partial x}\left(x^4\frac{\partial \bar{n}}{\partial x}\right) \tag{4.4}$$

Since the incident radiation is only weakly scattered, an approximate solution to 4.4 can be found by substituting the occupation number of a Planckian radiation field:

$$\bar{n_p}(x) = \frac{1}{e^x - 1}. \tag{4.5}$$

This makes the spectral form of the thermal Sunyaev-Zel'dovich effect

$$g(x) = \frac{x^4 e^x}{(e^x - 1)^2}\left[\frac{x(e^x + 1)}{e^x - 1} - 4\right]. \tag{4.6}$$

Therefore, different frequency maps need to be scaled differently in order to account for the frequency of the photons incident on the gas.

4.2 CMB Signal

The method for constructing a map of the Sunyaev-Zel'dovich effect is given by variants on the 'Internal Linear Combination' (ILC) method (Remazeilles et al., 2011). This method presumes very little about the form of the maps themselves, assuming that the maps can be written in the form

$$\vec{x}(p) = \vec{a}s(p) + \vec{n}(p) \tag{4.7}$$

where $\vec{x}$ is a vector of N_{obs}observations, $s(p)$ is a single map, $\vec{a}$ is a mixing vector, which does not depend on p but is known, and $\vec{n}$ is some noise term, containing both instrument and astrophysical noise. It is also assumed that the maps are the same resolution.

The method then provides an estimator of the mean map, $\hat{s_{ILC}}(p)$ of the map s, by making a linear combination $\hat{s}(p) = \vec{w}\vec{x}(p)$:

$$\hat{s_{ILC}} = \frac{\vec{a}^t \hat{R^{-1}}}{\vec{a}^t \hat{R^{-1}}\vec{a}}\hat{x} \tag{4.8}$$

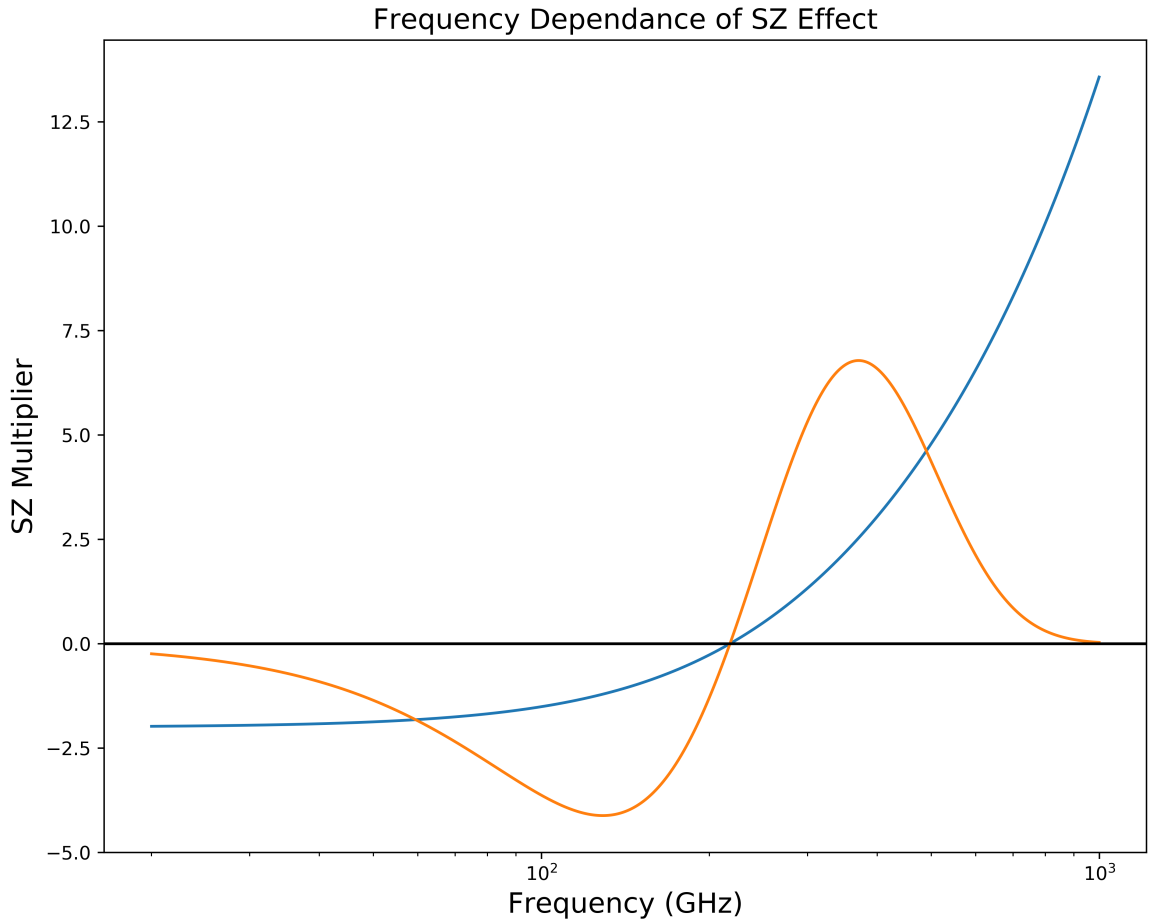

Figure 4.2: Sunyaev-Zel'dovich effect Intensity and Frequency Scaling Factors

where $\hat{R}$ is the covariance matrix of the observations.

This method then allows for the map to essentially be linearly added together, in such a way the the variance is minimised, and so the resulting map is as close to the best fit as possible.

One main advantage of the ILC component separation method is that it doesn't assume a model for the components that are not under direct consideration, they are simply collected in a catch-all nusiance term $\vec{n}(p)$. Unfortunately, if any of these components are correlated with the signals we are looking for, this method is unable to directly separate the signal from the noise without some *a priori* knowledge of the components a_i.

An updated version of the algorithm, known as the modified internal linear combination algorithm (MILCA) (Hurier et al., 2013), takes into account three changes to the above methodology. It accounts for localisation in pixel and spherical harmonic spaces to take into account and variations in spatial spectral laws. It also modifies the definition of the variance being minimised by an action of the covariance matix, to account for the possible correlation between noise and astrophyiscal sources.

Now, this technique can be applied to both the CMB as a whole, as well as the Sunyaev-Zel'dovich effect specifically.

The size of the anisotropy caused by the Sunyaev-Zel'dovich effect can be determined from the number of clusters sampled from the observational beam. This number is highly dependant on the constraints on cluster evolution and their subsequent properties. The range of angular scales depends on the angular extent of the clusters, but ultimately sits within ranges of approximately $1' - 10'$, for a typical cluster with a radial extent of approximately $0.5h_{-1}$Mpc, and a mass of $2 \times 10^{15} M_{\odot}$. For this system, we expect that the size of the anisotropy to be roughly $\Delta T/T \approx 10^{-6} - 10^{-5}$ (Rephaeli, 1995). This makes sense, since the upper measure for the total Comptonisation of the CMB is only 4×10^{-3}. However, it does pose an issue for detecting the WHIM, since the average density of a filament is so much lower than the density of a cluster. Given that the y parameter is sensitive to the temperature of the gas and the number density, reducing the number density by a factor of $10^5 - 10^8$ and the gas temperature by $\sim 10^2$, will result in a corresponding reduction in the measured y parameter.

Given the signal-to-noise ratio expected for the thermal Sunyaev-Zel'dovich effect of a single filament, many such filaments must be co-added, so as to drive the signal-to-noise to a detectable level. Initially outlined in Clampitt et al. (2016) for application to weak gravitational lensing maps, it was found that stacking ~ 135000 pairs yielded a filament mass at $\sim 4.5\sigma$ confidence. Further follow up using the Canada France Hawaii Telescope Lensing Survey (CFHTLenS), and the Sloan Digital Sky Survey's (SDSS) Luminous Red Galaxy (LRG) catalogue by Epps & Hudson (2017) detected the weak lensing signal from stacked filaments at 5σ confidence.

Investigations by Van Waerbeke et al. (2014), Ma et al. (2015), and Hojjati et al. (2015) established firmly that there is a correlation between weak gravitational lensing from CFHTLenS and tSZ signals from *Planck* , which suggests that we can use tSZ in the same way as weak lensing, without having to be careful about the peculiarities assosciated with weak lensing, such as sufficiently nulling spherical components. This was further reinforced by Hill & Spergel (2014), who reported a 6.2σ correlation between the *Planck* lensing potential and the *Planck* tSZ map.

Chapter 5

Stacking Methodology

Given the signal from a single filament is well below the level of noise in a given y map, in order to effectively detect the signal for the filaments, we need to add many individual sources together. Because the noise, and the signal in the CMB is presumed to be gaussian, the expectation is that correlated signals would add, and uncorrelated signals would be driven to zero. This means that by adding together thousands of signals lower than the signal-to-noise ratio of a given y map, it should show the filaments as a correlated signal, along with their corresponding galactic halos.

Initially outlined in Clampitt et al. (2016), the stacking algorithm involves creating a list of galaxy pairs, which we would expect to see a filament between, and then using those pairs, forming a normalised two-dimensional image, with the galaxies of the pair being placed on two points in the image, and stacking them until the signal to noise is sufficient to be measurable.

The intial problem faced involves generating the galaxy pairs from the Dark Energy Survey redMaGiC Catalogue. The Year 1 Catalogue consists of 0.65 million red-sequence galaxies in the redshift range $0.15 < z < 0.9$. The algorithm used by the Dark Energy Survey to select these red-sequence galaxies provides redshift estimates of very high quality and very low bias ($\lesssim 0.5$ percent). They also have very low scatter, and a very low rate of catastrophic outliers. The algorithm yields superior photo-z performance than the colour-cut methodology used to define the Sloan Digital Sky Survey CMASS catalogue (Rozo et al., 2016).

The DES catalogue has a larger footprint than the SPTpol viewing footprint, so we first have to exclude any galaxies that lie outside of the SPTpol area. The SPTpol observing area consists of a 500 square degree patch of sky, extending from an Right Acension (RA) of 22h to 2h, and a Declination (Dec) of -52 degrees to -67 degrees. Excluding any galaxies outside this region yields approximately 100000 galaxies, less than a sixth of the original catalogue.

Pairs were generated by making use of kD-trees. A generalisation of a binary tree, the kD tree is one where every leaf node is representative of a k dimensional point. Each non-leaf node is one that 'splits' the space into two parts, whereby points to the left of this hyperplane are represented by the left sub-tree, and to the right are represented by the right sub-tree. When we apply this to our galaxy catalogue, we first locate them in 3 dimensional space, by converting their RA, Dec, and redshift into a comoving 3D coordinate. They are then placed in a kD tree, and any pair which has a radial comoving separation of less that $10h^{-1}$ Mpc, and transverse comoving separation range of $6 - 14h^{-1}$ Mpc is considered to have a filament (Clampitt et al., 2016).

From this, approximately 340,000 galaxy pairs were constructed with a mean angular separation of ~ 31.6 arcmins, and a mean comoving separation of $11.9h^{-1}$ Mpc.

Figure 5.2 shows the overall distribution of galaxy pairs as a function of redshift. It shows that the mean redshift for the pairs is $z = 0.468$, with a minumum redshift of $z = 0.150$, and a maximum

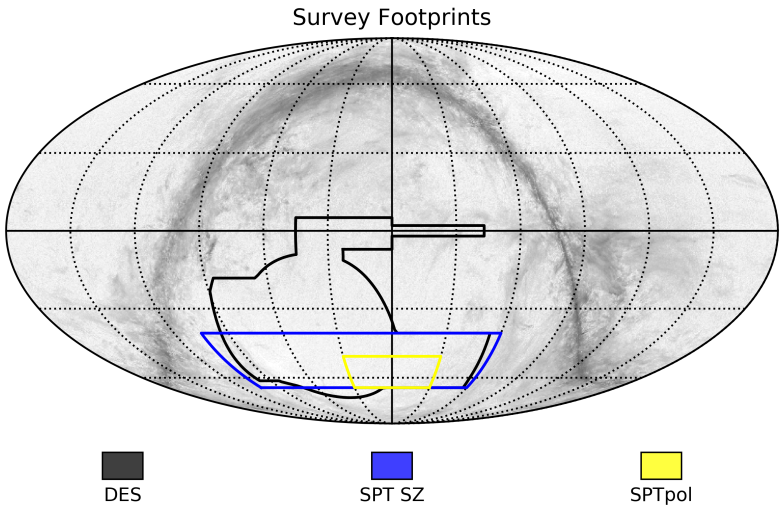

Figure 5.1: Outlines of SPTpol, SPT-SZ, and DES surveys

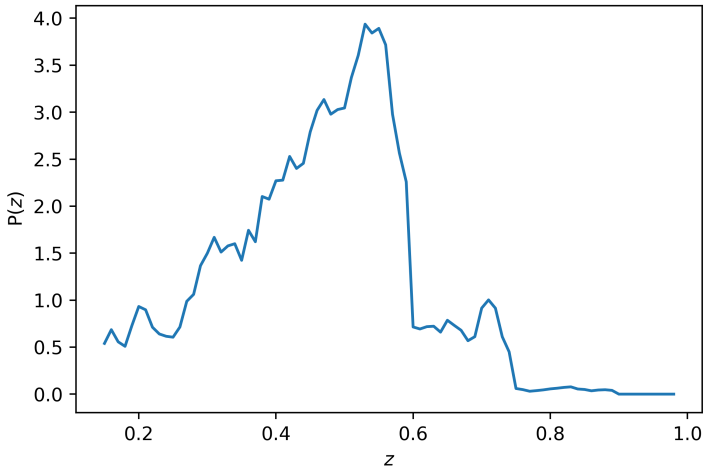

Figure 5.2: Redshift Distribution of Galaxy Pairs

redshift of $z = 0.899$. There is a rather drastic drop in the galaxy population after redshift $z \sim 0.58$. This is due to there being fewer galaxies in the higher redshift bins in the DES Year 1 Catalgogue.

Functionally, this means that the pair is located in the CMB, and a cutout of the CMB is taken around them, shown in Figure 5.3. We can see that this shows features we expect to see in the CMB, within characteristic ranges, and with a y-parameter measure given by the color bar.

They are then rotated, so they are all aligned along the same axis. This is done by applying an affine transformation to the array of values, because we are seeking to preserve the functional position of all points, straight lines, and ratios in the array, as close to the original as possible.

This subsequent image is then rescaled, so that each pair is located at the same point in the image.

Now that the pair has been rescaled and rotated correctly, we slice around the centre of the array, given that the two galaxies in a given pair have been positioned on the same points.

Now that the galaxy pair has been aligned, we calculate an average of the array, flipped along

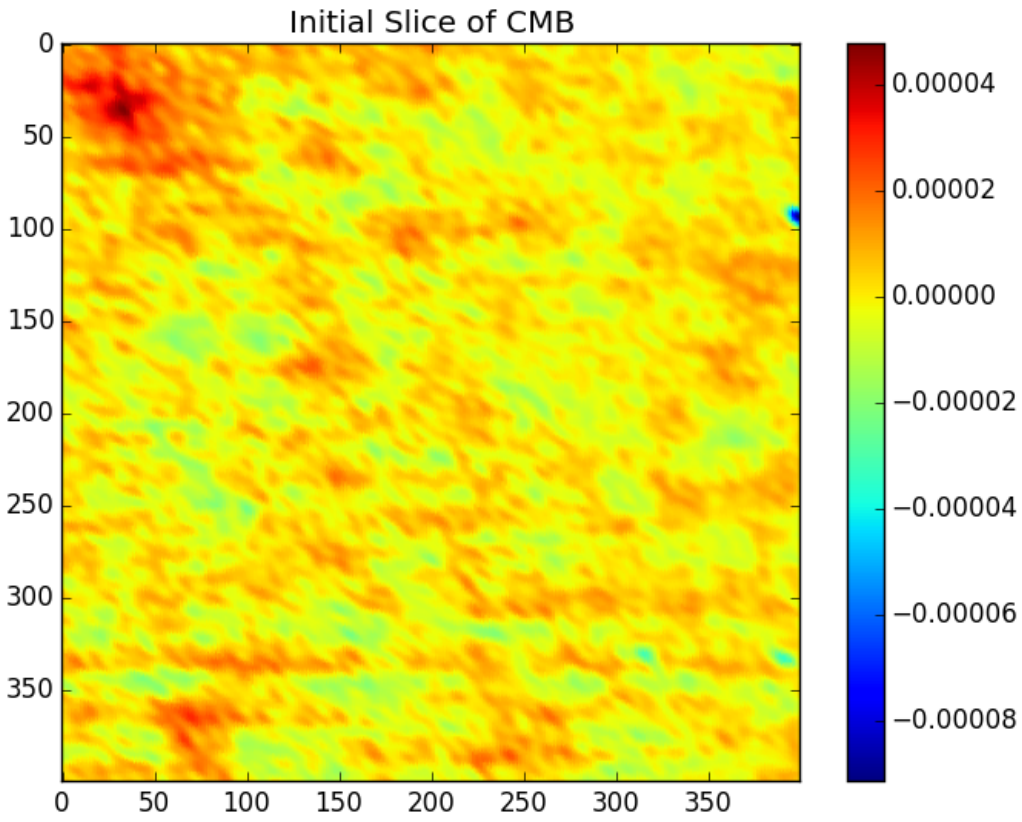

Figure 5.3: Initial Slice of CMB

both the x and y axes.

We do this in an effort to force the halos to be spherically symmetric.

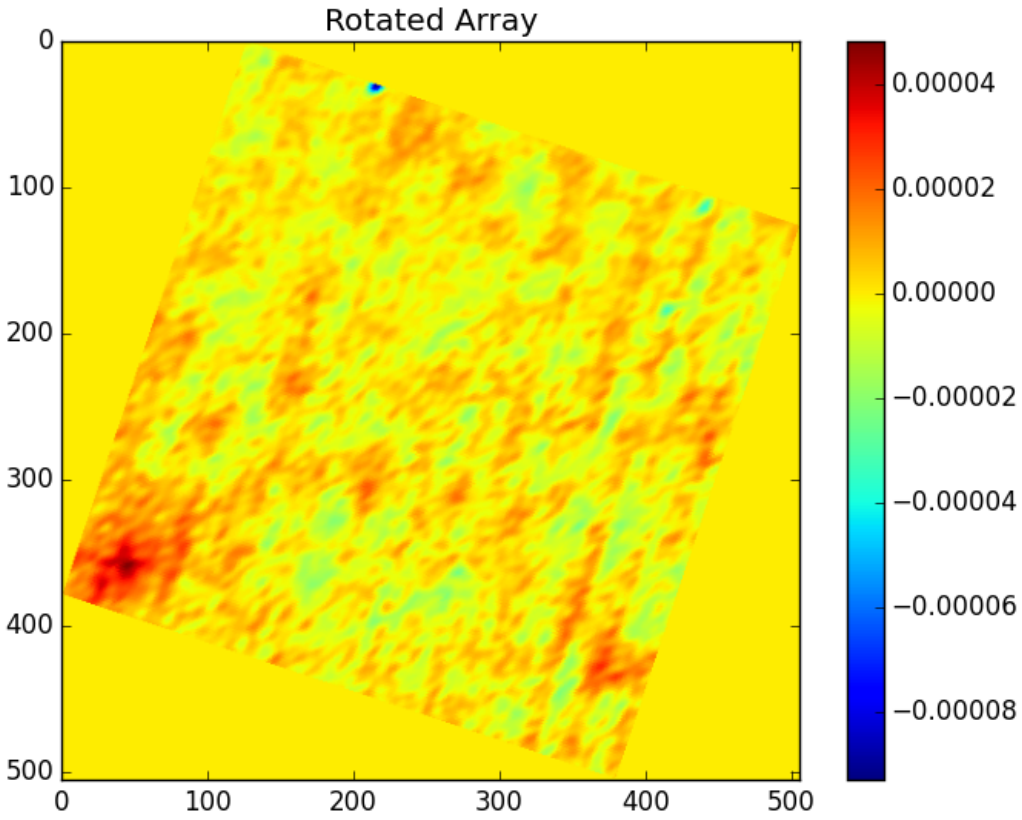

Figure 5.4: Rotated Cut-Out

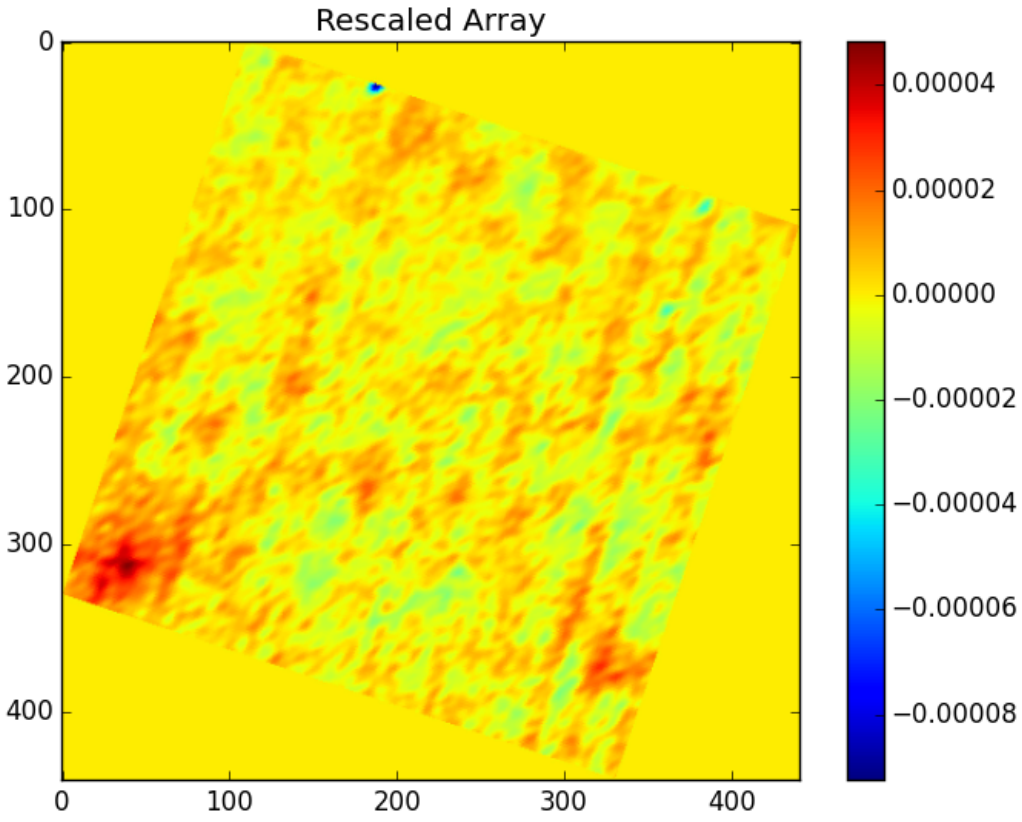

Figure 5.5: Rescaled Cut-Out

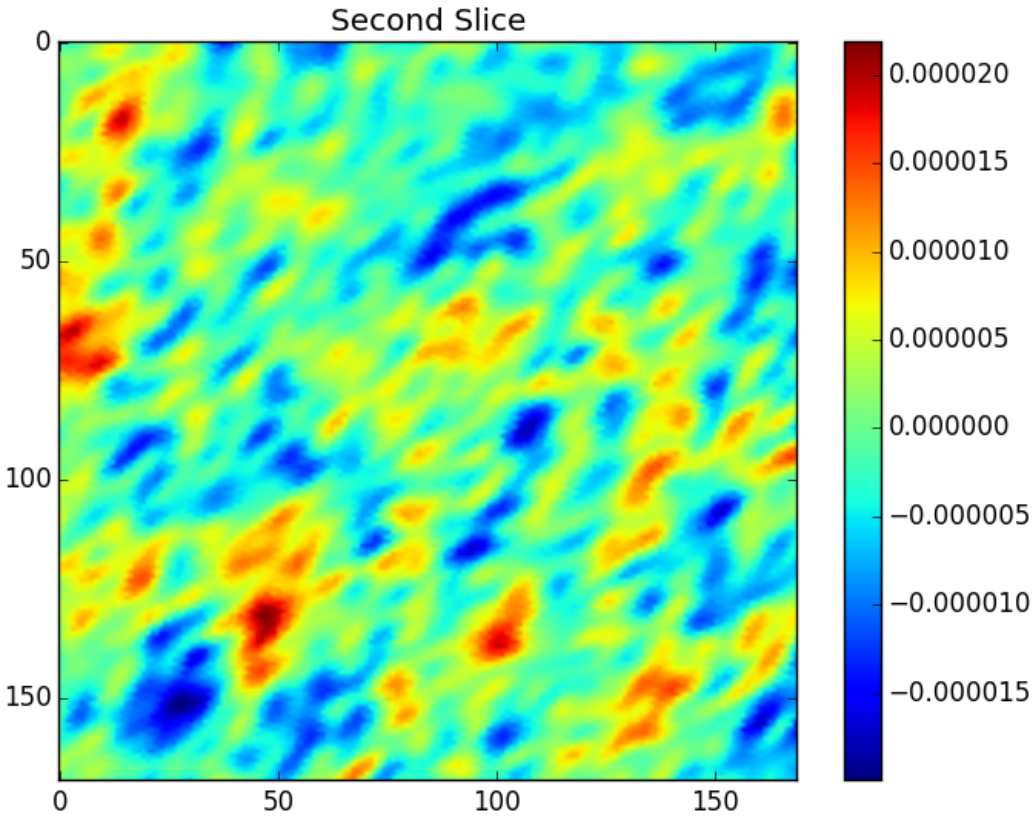

Figure 5.6: Second Cut-Out

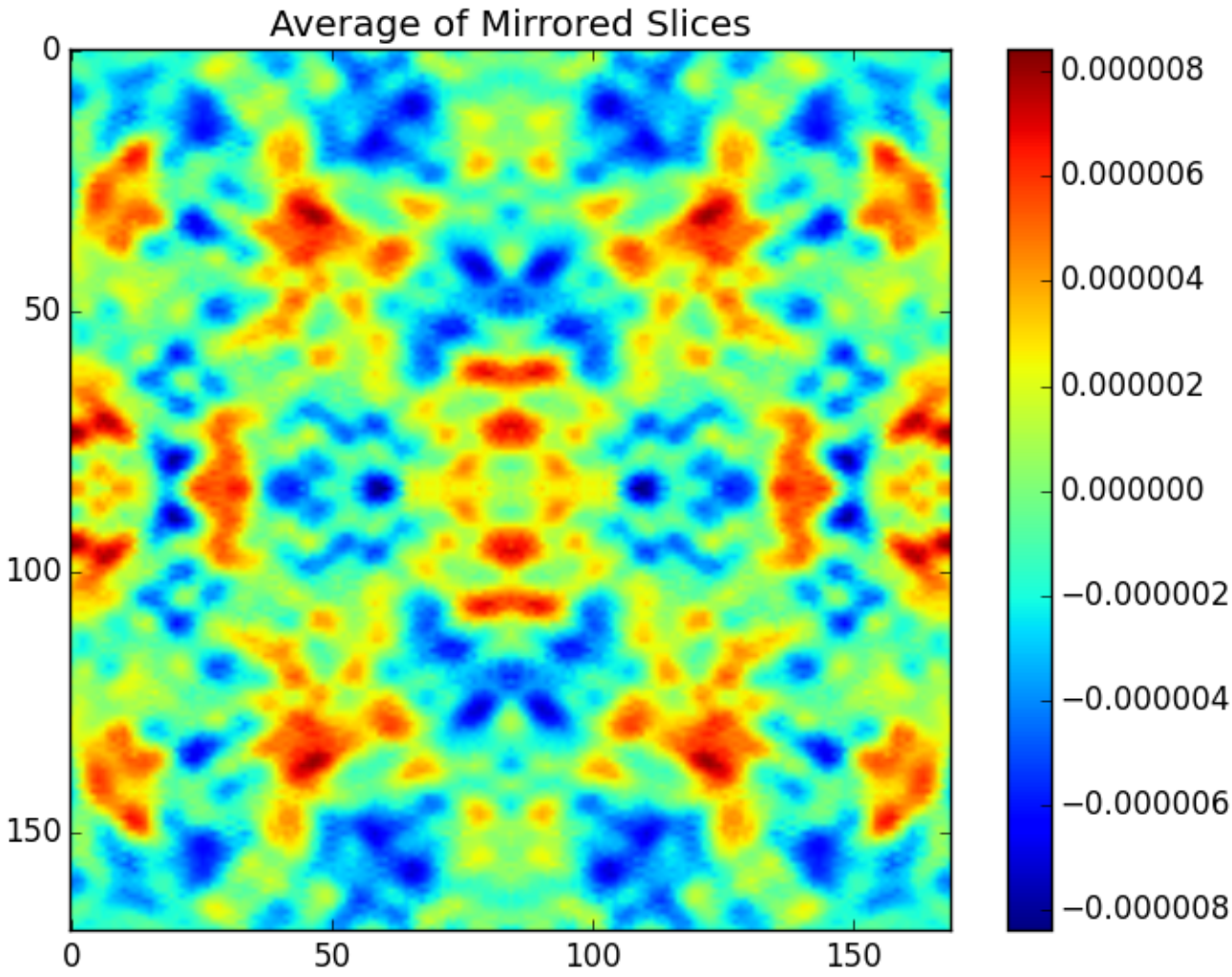

Figure 5.7: Average of Mirrored Arrays

Chapter 6

Results

Chapter 7

Conclusion

All your Concluding.

Bibliography

Bristow, P. D. & Phillipps, S., 1994, On the Baryon Content of the Universe, *MNRAS* 267, 13

Burles, S. & Tytler, D., 1998, Measurements of the deuterium abundance in quasar absorption systems, in Mezzacappa, A., editor, *Stellar Evolution, Stellar Explosions and Galactic Chemical Evolution*, p. 113

Cen, R. & Fang, T., 2006, Where Are the Baryons? III. Nonequilibrium Effects and Observables, *ApJ* 650, 2, 573

Cen, R. & Ostriker, J. P., 1999, Where Are the Baryons?, *ApJ* 514, 1, 1

Cen, R. & Ostriker, J. P., 2006, Where Are the Baryons? II. Feedback Effects, *ApJ* 650, 2, 560

Clampitt, J.; Miyatake, H.; Jain, B. & Takada, M., 2016, Detection of stacked filament lensing between SDSS luminous red galaxies, *MNRAS* 457, 3, 2391

Compton, A. H., 1923, A Quantum Theory of the Scattering of X-rays by Light Elements, *Physical Review* 21, 5, 483

Danforth, C. W. & Shull, J. M., 2005, The Low-z Intergalactic Medium. I. O VI Baryon Census, *ApJ* 624, 2, 555

Danforth, C. W. & Shull, J. M., 2008, The Low-z Intergalactic Medium. III. H I and Metal Absorbers at z < 0.4, *ApJ* 679, 1, 194

Davé, R.; Cen, R.; Ostriker, J. P.; Bryan, G. L.; Hernquist, L.; Katz, N.; Weinberg, D. H.; Norman, M. L. & O'Shea, B., 2001, Baryons in the Warm-Hot Intergalactic Medium, *ApJ* 552, 2, 473

Epps, S. D. & Hudson, M. J., 2017, The Weak Lensing Masses of Filaments between Luminous Red Galaxies, *MNRAS* 468, 3, 2605

Fukugita, M.; Hogan, C. J. & Peebles, P. J. E., 1998, The Cosmic Baryon Budget, *ApJ* 503, 2, 518

Fukugita, M. & Peebles, P. J. E., 2004, The Cosmic Energy Inventory, *ApJ* 616, 2, 643

Hill, J. C. & Spergel, D. N., 2014, Detection of thermal SZ-CMB lensing cross-correlation in Planck nominal mission data, *J. Cosmology Astropart. Phys.* 2014, 2, 030

Hojjati, A.; McCarthy, I. G.; Harnois-Deraps, J.; Ma, Y.-Z.; Van Waerbeke, L.; Hinshaw, G. & Le Brun, A. M. C., 2015, Dissecting the thermal Sunyaev-Zeldovich-gravitational lensing cross-correlation with hydrodynamical simulations, *J. Cosmology Astropart. Phys.* 2015, 10, 047

Hurier, G.; Macías-Pérez, J. F. & Hildebrandt, S., 2013, MILCA, a modified internal linear combination algorithm to extract astrophysical emissions from multifrequency sky maps, *A&A* 558, A118

Kompaneets, A. S., 1957, The Establishment of Thermal Equilibrium between Quanta and Electrons, *Soviet Journal of Experimental and Theoretical Physics* 4, 5, 730

Ma, Y.-Z.; Van Waerbeke, L.; Hinshaw, G.; Hojjati, A.; Scott, D. & Zuntz, J., 2015, Probing the diffuse baryon distribution with the lensing-tSZ cross-correlation, *J. Cosmology Astropart. Phys.* 2015, 9, 046

Penton, S. V.; Shull, J. M. & Stocke, J. T., 2000, The Local Lyα Forest. II. Distribution of H I Absorbers,Doppler Widths, and Baryon Content, *ApJ* 544, 1, 150

Penton, S. V.; Stocke, J. T. & Shull, J. M., 2004, The Local Lyα Forest. IV. Space Telescope Imaging

Spectrograph G140M Spectra and Results on the Distribution and Baryon Content of H I Absorbers, *ApJS* 152, 1, 29

Penzias, A. A. & Wilson, R. W., 1965, A Measurement of Excess Antenna Temperature at 4080 Mc/s., *ApJ* 142, 419

Persic, M. & Salucci, P., 1992, The baryon content of the universe, *MNRAS* 258, 1, 14P

Planck Collaboration; Aghanim, N.; Akrami, Y.; Ashdown, M.; Aumont, J.; Baccigalupi, C.; Ballardini, M.; Banday, A. J.; Barreiro, R. B. & Bartolo, N., 2018, Planck 2018 results. VI. Cosmological parameters, *arXiv e-prints* arXiv:1807.06209

Rao, S. & Briggs, F., 1993, Neutral Hydrogen in Galaxies at the Present Epoch, *ApJ* 419, 515

Remazeilles, M.; Delabrouille, J. & Cardoso, J.-F., 2011, CMB and SZ effect separation with constrained Internal Linear Combinations, *MNRAS* 410, 4, 2481

Rephaeli, Y., 1995, Comptonization Of The Cosmic Microwave Background: The Sunyaev-Zeldovich Effect, *ARA&A* 33, 541

Richter, P.; Savage, B. D.; Sembach, K. R. & Tripp, T. M., 2006, Tracing baryons in the warm-hot intergalactic medium with broad Ly α absorption, *A&A* 445, 3, 827

Rozo, E.; Rykoff, E. S.; Abate, A.; Bonnett, C.; Crocce, M.; Davis, C.; Hoyle, B.; Leistedt, B.; Peiris, H. V.; Wechsler, R. H. et al., 2016, redMaGiC: selecting luminous red galaxies from the DES Science Verification data, *MNRAS* 461, 2, 1431

Schaye, J., 2001, Model-independent Insights into the Nature of the Lyα Forest and the Distribution of Matter in the Universe, *ApJ* 559, 2, 507

Smith, B. D.; Hallman, E. J.; Shull, J. M. & O'Shea, B. W., 2011, The Nature of the Warm/Hot Intergalactic Medium. I. Numerical Methods, Convergence, and O VI Absorption, *ApJ* 731, 1, 6

Spergel, D. N.; Bean, R.; Doré, O.; Nolta, M. R.; Bennett, C. L.; Dunkley, J.; Hinshaw, G.; Jarosik, N.; Komatsu, E.; Page, L. et al., 2007, Three-Year Wilkinson Microwave Anisotropy Probe (WMAP) Observations: Implications for Cosmology, *ApJS* 170, 2, 377

Steigman, G., 2007, Primordial Nucleosynthesis in the Precision Cosmology Era, *Annual Review of Nuclear and Particle Science* 57, 1, 463

Van Waerbeke, L.; Hinshaw, G. & Murray, N., 2014, Detection of warm and diffuse baryons in large scale structure from the cross correlation of gravitational lensing and the thermal Sunyaev-Zeldovich effect, *Phys. Rev. D* 89, 2, 023508

Weinberg, D. H.; Miralda-Escudé, J.; Hernquist, L. & Katz, N., 1997, A Lower Bound on the Cosmic Baryon Density, *ApJ* 490, 2, 564

Wright, E. L., 2004, Theoretical Overview of Cosmic Microwave Background Anisotropy, in Freedman, W. L., editor, *Measuring and Modeling the Universe*, p. 291

Zwaan, M. A.; Staveley-Smith, L.; Koribalski, B. S.; Henning, P. A.; Kilborn, V. A.; Ryder, S. D.; Barnes, D. G.; Bhathal, R.; Boyce, P. J.; de Blok, W. J. G. et al., 2003, The 1000 Brightest HIPASS Galaxies: The H I Mass Function and Ω_{HI}, *AJ* 125, 6, 2842